geoconvention
Calgary • Canada • May 15-17 2023

How rock physics, saturation-height modelling and inversion attributes can help resolve the permeability structure – an example from a fluvio-marine sandstone reservoir

Draga Talinga, P. Geo, Geophysicist

Summary

This study investigates a practical cross-disciplinary technique for mapping reservoir permeability using hybrid templates generated from the combination of rock-physics modelling and core permeability expressed as a function of porosity and shale volume. The method is applied to characterize the permeabilities within the Hugin Formation sandstones at the Volve field using elastic properties estimated from seismic inversion. The interpretation of high permeability facies is also guided by the shift between the bulk volume of water (BVW) log and a field-derived BVW-height function. Results suggest that the method correctly identifies the highly permeable Middle Hugin layer and can provide important information on the subsurface permeability structure.

Method

Permeability is the ability of a rock to allow the movement of fluids through its pore system. However, permeability is one of the most difficult properties to characterize because it cannot be measured directly by geophysical methods. Still, to identify the flow barriers and guide the location of the wells, it is important to understand how it varies within the reservoir.

This paper describes a partly empirical workflow for identifying permeability variations by linking permeability with elastic properties through rock physics, evaluating the BVW, and regression analysis of core permeability with log porosity and shale volume. The method was tested on the North Sea Jurassic sandstones of the Hugin Formation to map 3D seismic data attributes into lithology and permeability facies. The Hugin Formation is a shallow marine sandstone with fluvio-deltaic influences, and it has a very heterogenous permeability. Samples with similar porosities, situated within one meter, showed significant shifts of more than two orders of magnitude difference in permeability (Statoil, 1993).

1) Rock-physics modelling

Through rock-physics models, various geological reservoir properties, such as porosity, mineralogy, and saturation, can be connected to seismic properties, such as P- and S-impedances or density. When constrained by local known or assumed geological factors, the rock physics models can help us avoid interpretation ambiguities that sometimes occur between sand and shale, porosity and saturation, or lithology and fluids (Avseth, 2010).

A rock physics model was calibrated to the Hugin reservoir using the constant-cement sand model (Dvorkin and Nur, 1996) and used to estimate the bulk and shear moduli of the porous dry frame. The properties of pore fluids were calculated based on their composition and in-situ temperature and pressure (Batzle and Wang, 1992). Lastly, fluid substitution (Gassmann, 1951) was used to account for pore fluid effects and predict the effective properties of the saturated sand. This model was used to create rock-physics templates covering various scenarios of clay volume and porosity to anticipate the expected changes that can occur away from the wells. Figure 1 shows the model plotted as density versus MuRho, properties which we can then use to interpret high-, medium-

and low-porosity sandstones. More details on the rock physics and the main lithology classification were previously discussed in Talinga and Reine (2021).

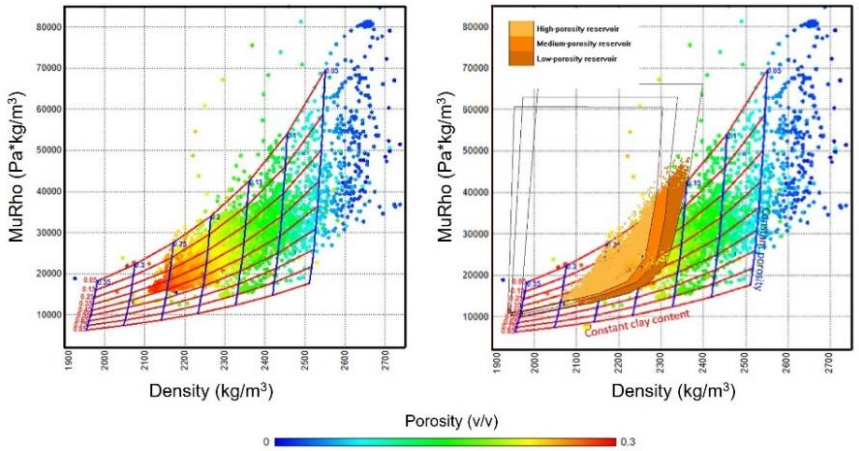

Figure 1. Crossplots to classify different reservoir facies. The rock physics template and well data (left) are shown with classified seismic points (right).

2) Adding permeability to rock physics templates

A continuous permeability log was calculated from multivariable regression analysis between porosity and shale volume logs against overburden-corrected core permeability. This relationship (Statoil, 2018), was also applied to the porosity and shale values of the rock-physics model, allowing for the new quantity to be plotted on the templates. The separation of low and high permeabilities is best observed on rock physics templates of porosity, clay volume and permeability displayed on Vp/Vs and density crossplots (Figure 2).

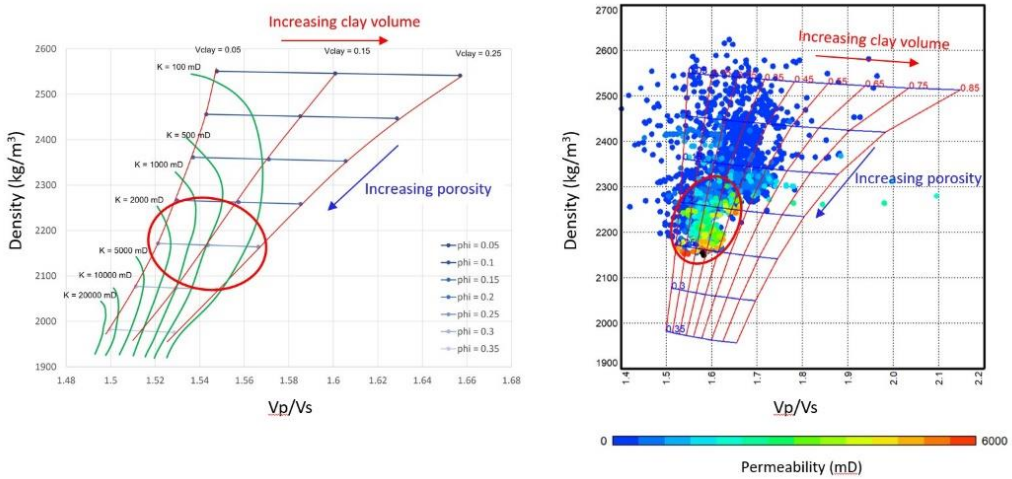

Figure 2. Crossplot templates showing variations in porosity, clay volume and permeability, expressed in density and VpVs ratio. Green lines indicate constant permeability calculated from the relationship between core permeability and log porosity and shale volume (left). Well data points displayed on porosity and clay volume templates and coloured by log permeability (right). High permeabilities are highlighted in red.

Although the templates show that high permeabilities correspond, as expected, to high porosities and small clay volumes, the well data contain variations in porosity and facies which results in a similar but not identical trend. While the introduction of permeability in the rock physics templates is useful, it becomes less reliable in the presence of rapid changes between sand and shale. Obtaining a good correlation between core and log permeability in these cases may be difficult because of possible poor correlations with porosity and shale fractions.

3) Cross-validation with BVW

Whichever method we use to characterize variations in a property, it is always important to check the results against other independent data sources. In this case, the results were compared with observed deviations between the calculated BVW log and the fitted trend above the free water level (the BVW-height function, or fractal function (Cuddy, 1993)).

BVW is the volume of capillary-bound water in the rock (Figure 3) and is calculated as the product of porosity and saturation. Because it quantifies the pore geometry, determined by the particles' size, shape, and arrangement, it is connected to both permeability and porosity.

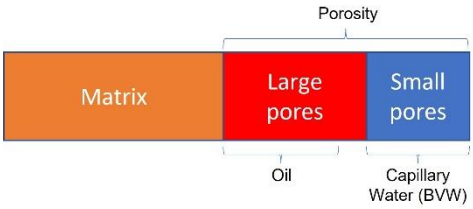

Figure 3. The bulk volume of water – generalized representation.

The BVW-height function predicts the volume of water as a function of height above the free water level (FWL). The function shows how the formation porosity is divided between hydrocarbon and water and is calculated from the height above the FWL, H, and two constants, a and b (Cuddy, 2017):

$BVW = a\ H^{b}$

Using the BVW trend obtained by plotting the BVW against the true vertical depth, the FWL was identified at 3200 m for one of the wells. Next, the parameters of the fractal function were calculated by linear regression on logarithmic scales plot of BVW against height above FWL:

$BVW = 0.153\ H^{-0.369}$

Only the best data was used, free of boundary effects, such as the middle of massive clean layers. When comparing the log- with the field-derived BVW (Figure 4), we can see that the field function overpredicts BVW in some of the beds, which indicates that these beds have a different porosity-permeability relationship compared to the other facies. As a consequence, the log-derived BVW is shifted in these beds. The highly permeable beds stand out as having a much lower BVW compared to what the field-derived BVW function predicts. This method has been successfully used to predict highly permeable beds in the Buzzard field in the Central North Sea (S. Cuddy, personal communication, 2022).

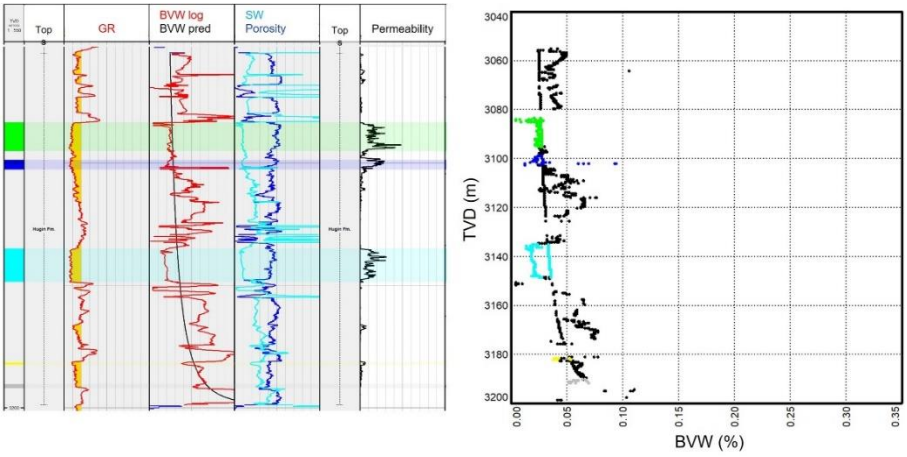

Figure 4. Petrophysical logs showing zones subdivided based on the shift between the BVW log and the best-fit BVW-height function in a well with a free water level at 3200 m (left). Comparison of log and field-derived BVW (right).

Figure 5 shows that, when combined with rock physics, the core-to-log high permeabilities are matched to the same degree by overestimations of the predicted BVW values. Here, the rock physics model is seen in the P-wave velocity versus density domain, as the well doesn't have a shear sonic log to calculate the VpVs ratio. The comparison suggests that the BVW function captures the high permeability beds and could be a workaround solution, particularly when core heterogeneity is strong.

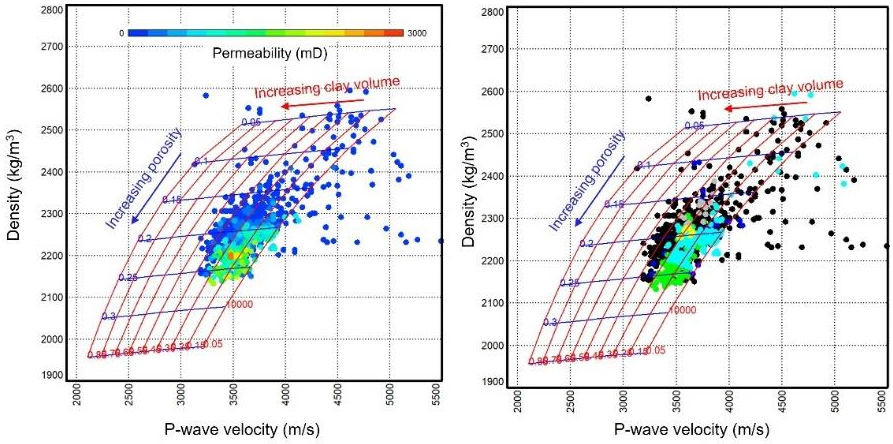

Figure 5. P-wave velocity log data versus density and superimposed rock physics model. On the left, data points are coloured by permeability, and on the right, by the highlighted high permeability beds. We can see that the match is very good, suggesting that BVW could be used as an indicator in the absence of permeability data.

4) 3D workflow application

The application within the 3D was realized by crossplotting the inverted seismic attributes to separate the main lithologies based on their difference in elastic properties. The reservoir sandstones were further classified into high permeability and low, medium, and high porosity sands using the rock-physics templates obtained for the constant-cement model. The

interpretation of permeability classes was guided by both the well log permeability and the identified shifts between the log and field-derived BVW.

A cross-section and a horizon slice through the reservoir show an excellent correlation between the high permeability facies and the permeability logs, which enabled imaging of the highly permeable Middle Hugin unit on the eastern flank of the structure (Figure 6). Localized areas of increased permeability in the east and southeast of the study area suggest lateral changes in the depositional environment.

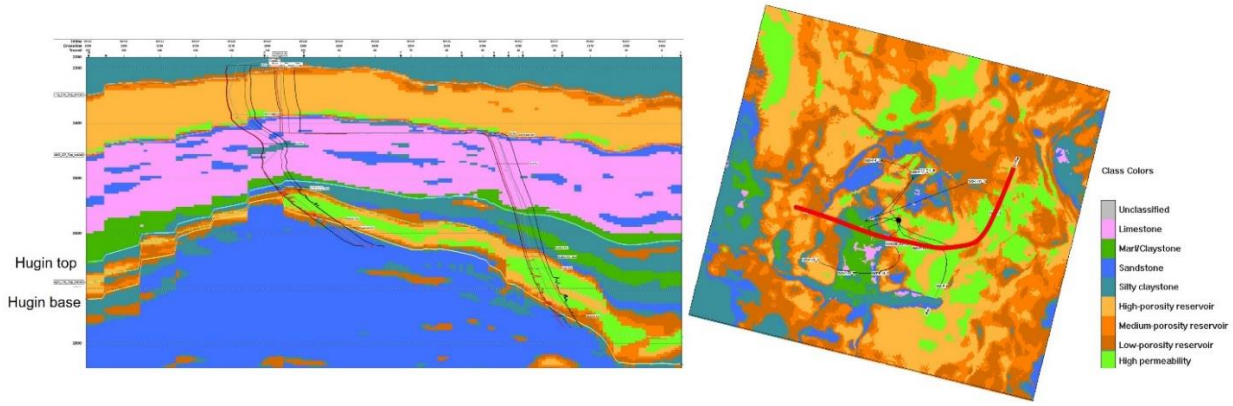

Figure 6. Classified seismic data is shown on vertical cross-section (red line) and horizon slice 30 ms above the reservoir base, showing the high porosity sands subdivided based on permeability. The permeability log is inserted in black to the right of the well trajectory.

Conclusions

A new method was proposed and applied for detecting high permeability facies within the Hugin reservoir by combining seismic, well and core data through rock physics, petrophysical evaluation and seismic inversion. Changes in mineralogy and porosity were modelled based on known reservoir conditions and a constant cement fraction calibrated to the reservoir. Core permeability expressed as a function of log porosity and shale volume allowed to substitute permeability in the model, create rock physics templates, and accurately identify permeability trends. The interpretation of highly permeable facies was also constrained by the associated shifts between the log- and field-derived BVW values above the free water level. The advantage of combining rock physics and inversion techniques with BVW modelling is that the BVW can assist in differentiating anomalous permeabilities in the 3D volume even when permeability measurements are not available.

Acknowledgements

Thanks to Equinor, ExxonMobil, Bayerngas, and the Norwegian Petroleum Directorate for making the Volve field dataset available. I am grateful for the support in this work by Laurie Weston and Carl Reine of Sound QI, and for the insightful guidance on the BVW-height modelling provided by Steve Cuddy. Special thanks to Alex Turta for inspiring me to explore this topic further.

References

Avseth, P. (2010). Exploration rock physics – the link between geological processes and geophysical observables, Chapter 18 in Petroleum Geoscience: From Sedimentary Environments to Rock Physics.
Batzle M, & Wang, Z. (1992). Seismic properties of pore fluids. Geophysics, 57(11), 1396-1408.
Cuddy, S. (1993). The Fractal function - a simple, convincing model for calculating water saturations in Southern North Sea gas fields: Transactions of the 34th Annual Logging Symposium of the SPWLA, Calgary, Canada.
Cuddy, S. (2017). Using fractals to determine a reservoir's hydrocarbon distribution, SPWLA 58th Annual Logging Symposium.
Dvorkin, J., & Nur, A. (1996). Elasticity of high-porosity sandstones: Theory for two North Sea data sets. Geophysics, 61, 1363-1370
Gassmann, F. (1951). Elastic waves through a packing of spheres: Geophysics, 16, 673-685.
Statoil. (1993). Discovery Evaluation Report, Well 15/9-19 SR, Theta Vest Structure.
Statoil. (2018). Sleipner Øst and Volve Model 2006, Hugin and Skagerrak Formation Petrophysical Evaluation.
Talinga, D., and Reine, C. (2021). Integrating pore pressure and lithology prediction from well and seismic data to characterize abnormal pressures in the compartmentalized Volve oil field, Central North Sea: CSEG Recorder, 46, no. 02.